Crystallization and preliminary X-ray analysis of twinned crystals of a chimeric FK506 binding protein 12 and 13 complexed with FK506

JUN LIANG,[a] STEVE EALICK,[b] CHRIS NIELSEN,[c] STUART L. SCHREIBER[d] AND JON CLARDY[a]* *at [a]Department of Chemistry and [b]Section of Biochemistry, Molecular and Cell Biology, Cornell University, Ithaca, New York 14853-1301, USA, [c]Department of Chemistry, University of California San Diego, La Jolla, California 92093, USA, and [d]Department of Chemistry, Harvard University, Cambridge, Massachusetts 02138, USA*

Abstract

An FKBP12/13 chimera with the 80s loop of FKBP13 replacing the corresponding loop in FKBP12 tightly binds the immunosuppressive agents FK506 and rapamycin and efficiently catalyzes peptidyl-prolyl *cis–trans* isomerization. However, the chimera's complex with FK506 does not inhibit calcineurin's phosphatase activity [Yang, Rosen & Schreiber (1993). *J. Am. Chem. Soc.* **115**(2), 819–820]. The chimeric protein crystallizes in space group *P*1 and the crystals are always twinned. The twin composites are related by a twofold twinning axis parallel to the *a* axis. A resolution data set (1.5 Å resolution) for a twinned crystal was collected at CHESS using 0.91 Å X-rays and image plates. Preliminary molecular replacement using data between 15 and 3 Å and the FKBP12–FK506 crystal structure as the search model led to a clear solution with a residual of 34.2%. This 3 Å resolution structure provides insight into the structural basis of twinning.

1. Introduction

FKBP12 was first isolated through its ability to selectively bind the potent immunosuppressive drug FK506 (Harding, Galat, Uehling & Schreiber, 1989; Siekierka, Hung, Poe, Lin & Sigal, 1989). Later work showed that the complex of FKBP12 with FK506, but neither component alone, binds to and inhibits the protein phosphatase calcineurin (Liu *et al.*, 1991). In resting helper T cells, this calcineurin inhibition prevents the translocation of the cytoplasmic subunit of the transcription factor NF-AT into the nucleus (Flanagan, Corthsy, Bram & Crabtree, 1991), thus blocking the signal transduction pathway for activation emanating from the T-cell receptor. Several other members of the FKBP family have also been described, including FKBP's of 13, 25 and 59 kDa (Jin *et al.*, 1991; Galat, Lane, Standaert & Schreiber, 1991; Tai, Albers, Chang, Faber & Schreiber, 1992). Even though FKBP13 has high sequence identity with FKBP12 (43%), and binds FK506 almost as tightly as FKBP12 (K_i = 55 *versus* 0.4 n*M*), the FKBP13–FK506 complex has a two order of magnitude lower affinity for calcineurin (K_i = 1500 *versus* 16 n*M*) (Yang *et al.*, 1993). In order to investigate the composite binding surface with which the FKBP12–FK506 complex inhibits calcineurin, mutagenesis studies based on both the NMR structure of FKBP12 (Michnick, Rosen, Wandless, Karplus & Schreiber, 1991) and the X-ray structure of the FKBP12–FK506 complex (Van Duyne, Standaert, Schreiber & Clardy, 1991) were conducted (Yang *et al.*, 1993; Rosen, Yang, Martin & Schreiber, 1993). Two external loops near the ligand binding site (designated as the 40s and 80s loops according to their numbering in FKBP12) were implicated in calcineurin binding, and several FKBP12/13 chimeras in which these loops were

interchanged were constructed (Yang *et al.*, 1993; Rosen *et al.*, 1993). In this paper, we report the crystallization and characterization of a FKBP12/13 chimera where the 80s loop of FKBP12 has been replaced by the corresponding region of FKBP13 (Yang *et al.*, 1993). Although only six amino acids have been changed [A(84)TGHPGI→ERGAPPK], this primarily FKBP12-like protein behaves like FKBP13 in terms of its inhibition of calcineurin (K_i = 580 n*M*). A comparison of its high-resolution structure with that of the native FKBP12–FK506 complex could provide useful insights into the binding selectivity of calcineurin.

2. Crystallization and X-ray analysis

FKBP12/13 chimera was constructed and purified as reported (Yang *et al.*, 1993), concentrated to 10 mg ml^{-1} (in 10 m*M* Tris, 10 m*M* DTT, pH 8.0), and then mixed with FK506 (at 10 mg ml^{-1} dissolved in MeOH) at a 3:1 molar ratio. Dithiothreitol (DTT) was added to inhibit the dimerization of the protein through the oxidation of a free cysteine residue on the surface. Since FK506 is sparingly soluble in water, uncomplexed FK506 precipitated out upon addition to the FKBP12/13 chimera solution. The mixture was vortexed gently, and then stored at 277 K overnight. The mixture was passed through a 0.22 μm filter unit (Millipore) to remove uncomplexed FK506 and any other contaminants before use. The hanging-drop method was used to set up the incomplete factorial crystallization screen (Carter, Baldwin & Frick, 1988). A total of 46 different combinations of crystallization conditions were sampled. Crystals appeared after 2 d using 1.6–1.8 *M* Na$_2$HPO$_4$/K$_2$HPO$_4$, 100 m*M* HEPES at pH 8.1. Most crystals showed either inclusion bodies or other facial defects.

The characterization of the space group was carried out using two San Diego Multiwire detector systems and graphite-monochromated Cu *K*α radiation from a Rigaku RU-200 rotating-anode source. The first zone (0*kl*) was identified easily. A simulated precession photograph revealed no mirror symmetry in the zone. Twinning became apparent during the search for other zones. Data from a 12° *ω*-oscillation were collected with the detector-to-crystal distances of 779 and 719 mm. A program was written to transform the data to a three-dimensional reciprocal lattice. The positions of these reflections in reciprocal space (in Protein Data Bank format) were viewed on a Silicon Graphics computer using *CHAIN* (Sack, 1988). This method clearly showed that the space group was triclinic and crystals were twinned. A total of 48 reflections belonging to one lattice were manually chosen and successfully indexed using the San Diego Multiwire system auto-indexing software (Howard,

Nielsen & Xuong, 1985). The cell parameters, as well as the orientation matrix, were refined against these reflections and gave $a = 35.3$ (2), $b = 36.8$ (2), $c = 49.6$ (2) Å, $\alpha = 102.0$ (5), $\beta = 92.2$ (5), $\gamma = 116.0$ (5)°. The total volume of the unit cell is 56 173.7 Å^3. Assuming two molecules in the asymmetric unit, the Matthews constant is 2.4 Å^3 Da^{-1}, which corresponds to 50% solvent content. The lattice could also be assigned to a pseudo-monoclinic $C2$ with $a' = 49.6$, $b' = 35.3$, $c' = 66.4$ Å, $\alpha = 87.0$, $\beta = 104.4$, $\gamma = 92.2°$. The relation between these two cells is $\mathbf{a}' = \mathbf{c}$, $\mathbf{b}' = \mathbf{a}$, $\mathbf{c}' = 2\mathbf{b} + \mathbf{a}$, and this metric coincidence is related to the pervasive twinning in these crystals (Buerger, 1945). A more fundamental insight into the twinning came when it was later shown that the two molecules in the asymmetric unit are related by a pseudo twofold ($\psi = 89.3$, $\varphi = 0.5$, $\kappa = 177.6°$ as defined by the *X-PLOR* program), which almost parallels the twinning law twofold.

Since every crystal examined showed the same twinning, we had no choice but to collect intensity data from a twinned crystal. As will be discussed shortly, the crystals showed non-merohedral twinning, *i.e.* the reciprocal lattices of the two twin components were in perfect registry in some and out of registry in other regions of reciprocal space. Data for a unique component of the twin could be collected in the regions where there was not perfect registry.

The zone of perfect registry for the FKBP12/13 chimera–FK506 complex is the $(0kl)$ zone – the twinning law is a twofold along the a axis. Therefore, the shortest distance between the diffraction maxima from the different lattices in each (nkl) zone is identical, and its magnitude depends solely on an integral value of n. A precession simulating program was written locally to determine the shortest distance for each (nkl) and the result was illustrated in Fig. 1. As illustrated, the diffraction maxima from two lattices separate and then converge periodically with the index h, and two lattices become almost coincident with each other on zones where $h = 13$, 14, 27 and so on. For example, the shortest reciprocal distances were 0.0024 Å^{-1} for $(1kl)$ zone and 0.0013 Å^{-1} for $(13kl)$ and $(14kl)$ zones, which correspond to real-space distances of 410 and 770 Å, respectively. To collect data with these long apparent axis lengths, the detectors were moved away from the crystal as far as possible (1165 and 1225 mm), and another set of 12 ω-oscillation data was collected. In this way, reflections from the $(1kl)$ were just barely resolved. Synchrotron radiation was chosen for the final data collection both to resolve reflections as much as possible and to obtain a higher resolution data set.
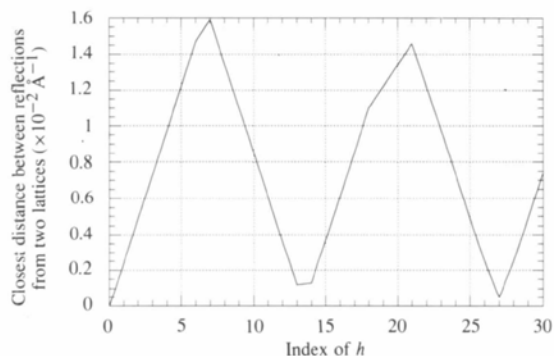
Table 1. *Data-collection statistics*

Resolution (Å)	No. measured	No. unique	R_{sym}*	Percent complete	No. with $F > 2\sigma$
99–4.3	2578	1432	0.133	89.2	1280
4.3–3.4	2500	1431	0.101	89.1	1277
3.4–3.0	2616	1444	0.084	90.0	1296
3.0–2.7	2495	1421	0.103	90.4	1278
2.7–2.5	2547	1430	0.096	89.5	1277
2.5–2.4	2481	1435	0.099	90.5	1283
2.4–2.3	1520	1426	0.102	91.7	1295
2.3–2.2	2561	1454	0.125	89.8	1280
2.2–2.1	2490	1439	0.137	90.4	1281
2.1–2.0	2468	1432	0.159	90.2	1251
All	25265	14344	0.110	90.1	12798

* $R_{sym} = \sum_{hkl} \sum_j |I_j(hkl) - \langle I(hkl) \rangle| / \sum_{hkl} \sum_j \langle I(hkl) \rangle$ where j runs over symmetry-related reflections.

Data were collected at the CHESS synchrotron F1 station using a wavelength of 0.91 Å, a 0.1 mm collimator, and a crystal-to-image-plate distance of 200 mm. The crystal diffracted beyond 1.5 Å at room temperature. A full data set was collected on 122 Fuji image plates with an oscillation angle of 2.0° and an exposure time of 10 s for each plate. The crystal was large enough (1.0 × 0.7 × 0.3 mm) to collect data at five different positions along the longest dimension of the crystal. At each position, 24 or 25 images were collected since the resolution limit increased to 2.0 Å after 25 images.

Separation of the twinned lattices and accurate measurement of the intensities of close reflections were the major challenges at this stage. Each image was carefully examined until one was found where the two lattices could be distinguished (Fig. 2). A unique lattice was manually indexed using *DENZO* (Z. Otwinowski, personal communication). A low-symmetry space group and small unit cell facilitated this step (Fig. 3). At the same time, auto-indexing for both lattices was successful using *REFIX* (Kabsch, 1993), and the matrices from *REFIX* and from *DENZO* agreed well. *DENZO* was chosen to measure the intensity of each
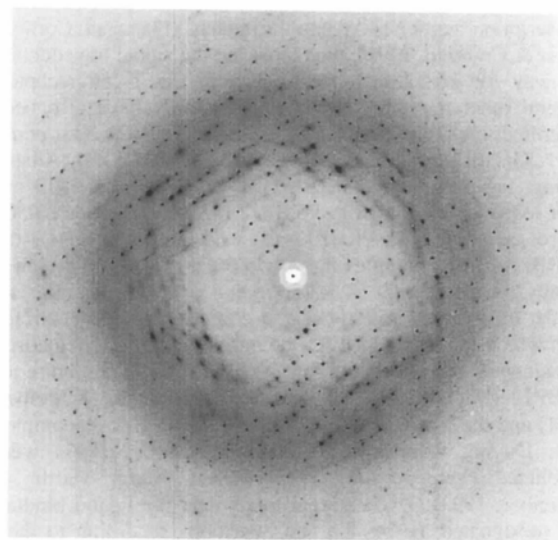

Fig. 2. The image that was used to separate the spots from two lattices using *REFIX*.

Fig. 1. The shortest distance between reflections from the two lattices is shown as a function of the index h of the reciprocal lattice.
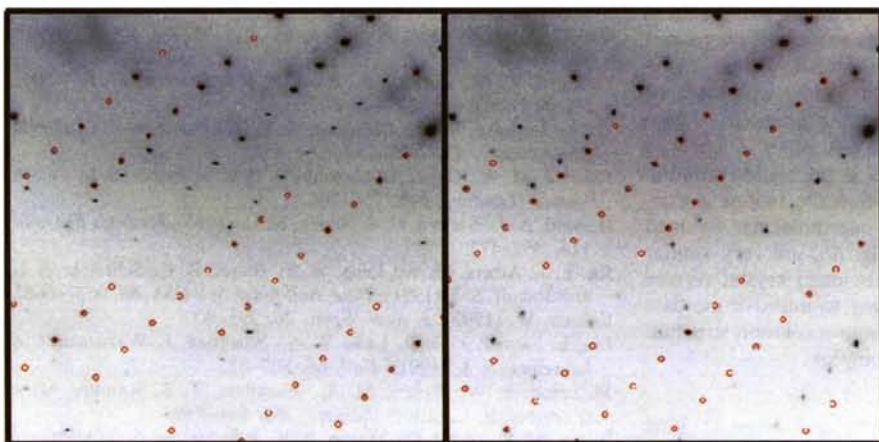
Fig. 3. An enlarged region of Fig. 2. The red circles are reflection positions predicted by *DENZO* from the given cell parameters and orientation matrix. Predictions of one lattice are shown on the left while predictions of the second lattice are shown on the right.

reflection because of its flexibility in handling the background calculations. This facility was required in order to minimize the effects of an adjacent reflection. Each reflection was judged by statistical values in terms of $\chi(x)^2$ and $\chi(y)^2$. A positional χ^2 value assumed a Gaussian distribution of intensity in x and y and was defined as the square of the observed error in the distribution divided by the square of the expected error in the distribution. The expected errors were counting statistics and the error parameters entered in the program $\{\chi(x)^2 = \sum[I_{\text{obs}}(x)^2 - I_{\text{cal}}(x)^2]^2/[\Delta I_{\text{obs}}(x)]^2,$ $\chi^2 = \chi(x)^2 + \chi(y)^2\}$. Perfect reflections should have $\chi(x)^2$ and $\chi(y)^2$ values close to 1.0. Reflections with relatively high χ^2 values were either very close to a reflection from the second lattice or highly overloaded. A data set belonging to one lattice was reduced with five runs of 122 images. An initial run of data from 24 images belonging to the second lattice was also reduced. Approximately, 10% of the observations show χ^2 greater than 9.0, and at this stage, they have not been rejected. Data were scaled and merged by *SCALEPACK* (Z. Otwinowski, personal communication) to 2.0 Å at present, and the data-reduction statistics are summarized in Table 1. The ultimate goal of data reduction is to find an objective way to 'detwin' the lattices and to minimize the interference on intensity measurement from the adjacent lattice for all non-overlapped reflections.

3. Molecular replacement

In order to check the preliminary data analysis, a molecular-replacement search was initiated using the data between 15 and 3 Å. Both molecules were positioned in the cell using *X-PLOR* (Brünger, 1993) and the native FKBP12-FK506 structure as a search model (Van Duyne *et al.*, 1991). Rigid-body refinement yielded a residual factor of 34.2% for the current data. The non-crystallographic pseudo twofold ($\upsilon = 89.3$, $\varphi = 0.5$, $\kappa = 177.6°$ defined by *X-PLOR*) which relates the independent molecules, is parallel to the twinning twofold ($\upsilon = 90.0$, $\varphi = 0.0°$). The packing of an ideal (untwinned) crystal looking down the *a* axis is shown in Fig. 4(*a*). Two molecules in an asymmetric unit are drawn in thin and thick lines respectively, and both the non-crystallographic pseudo twofold axis relating to two independent complexes and the twinning twofold are perpendicular to the plane of the figure. The packing shown
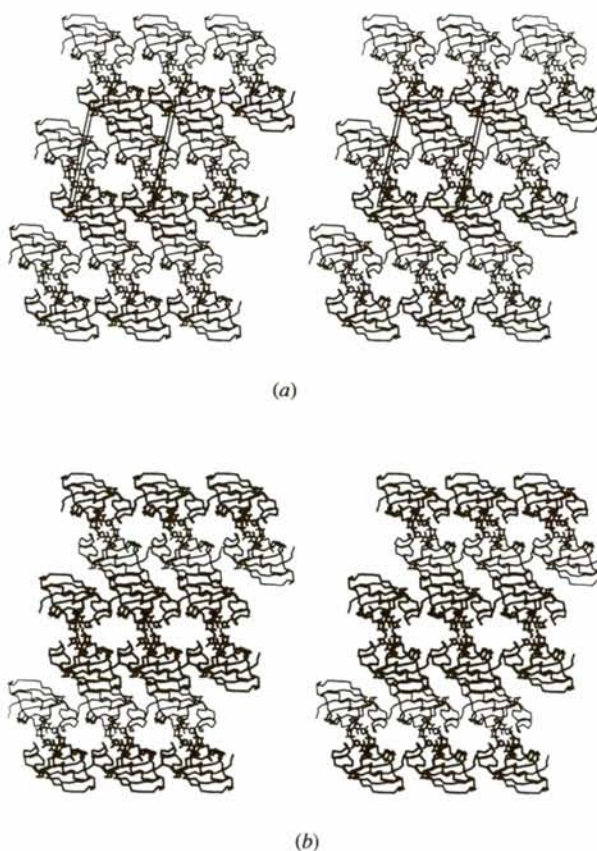

(*a*)

(*b*)

Fig. 4. (*a*) A packing diagram of an ideal (untwinned) crystal looking down the *a* axis. Protein molecules are drawn in Cα tracing and the ligand in a stick convention. The complexes which are related by the non-crystallographic twofold are drawn in thin and thick lines, respectively. The box represents the unit cell. Both the twinning twofold axis and the non-crystallographic twofold are perpendicular to the plane of the paper. (*b*) Hypothetical twinned lattice with the same view as (*a*). The twinning twofold axis coincides with the non-crystallographic twofold axis. The difference between (*a*) and (*b*) is in the center of each figure where a row of thin and thick molecules interact in (*a*) while rows of thick molecules interact in (*b*).

in Fig. 4(a) also explains the pervasive twinning seen in these crystals. The two molecules in the asymmetric unit are related by a pseudo twofold and a translation of 5.6 Å along the a axis. Most likely the twinning twofold coincides with the non-crystallographic twofold, and the twinning arises as shown in Fig. 4(b). A translation of only 5.6 Å along a changes the non-crystallographic twofold plus a translation relating the molecules in an asymmetric unit into the twinning axis. As seen in Figs. 4(a) and 4(b), the intermolecular twinned contacts between lattices (center of Fig. 4b) are very similar to the crystal contacts in an ideal untwinned crystal (center of Fig. 4a). We are currently attempting to improve the data quality in order to obtain an accurate high-resolution structure of the FKBP12/13 chimera–FK506 complex.

References

Brünger, A. T. (1993). *X-PLOR Version 3.1, A System for X-ray Crystallography and NMR*. Yale University Press, New Haven, CT, USA.

Buerger, M. J. (1945). *Am. Mineral.* **30**, 469–482.
Carter, C. W., Baldwin, E. T. & Frick, L. (1988). *J. Cryst. Growth*, **90**, 60–73.
Flanagan, W. M., Corthsy, B., Bram, R. J. & Crabtree, G. R. (1991). *Nature (London)*, **352**, 803–807.
Galat, A., Lane, W. S., Standaert, R. F. & Schreiber, S. L. (1991). *Biochemistry*, **31**, 2427–2434.
Harding, M. W., Galat, A., Uehling, D. E. & Schreiber, S. L. (1989). *Nature (London)*, **341**, 758–760.
Howard, A. J., Nielsen, C. & Xuong, N. H. (1985). *Methods Enzymol.* **114**, 452–472.
Jin, Y. J., Albers, M. W., Lane, W. S., Bierer, B. E., Schreiber, S. L. & Burakoff, S. J. (1991). *Proc. Natl Acad. Sci. USA*, **88**, 6677–6681.
Kabsch, W. (1993). *J. Appl. Cryst.* **26**, 795–800.
Liu, J., Farmer, J. D. Jr, Lane, W. S., Friedman, J., Weissman, I. & Schreiber, S. L (1991). *Cell*, **66**, 807–815.
Michnick, S. W., Rosen, M. K., Wandless, T. J., Karplus, M. & Schreiber, S. L. (1991). *Science*, **252**, 836–839.
Rosen, M. K., Yang, D., Martin, P. K. & Schreiber, S. T. (1993). *J. Am. Chem. Soc.* **115**(2), 821–822.
Sack, J. S. (1988). *J. Mol. Graphics*, **6**, 224–225.
Siekierka, J. J., Hung, H. Y., Poe, M., Lin, C. S. & Sigal, N. S. (1989). *Nature (London)*, **341**, 755–757.
Tai, P. K., Albers, M. W., Chang, H., Faber, L. E. & Schreiber, S. L. (1992). *Science*, **256**, 1315–1318.
Van Duyne, G. D., Standaert, R. F., Schreiber, S. L. & Clardy, J. (1991). *Science*, **252**, 839–842.
Yang, D., Rosen, M. K. & Schreiber, S. L. (1993). *J. Am. Chem. Soc.* **115**(2), 819–820.